University of Huddersfield Repository

Zhao, Yunshi and Liang, Bo

Re-adhesion control for a railway single wheelset test rig based on the behaviour of the traction motor

Original Citation

Zhao, Yunshi and Liang, Bo (2013) Re-adhesion control for a railway single wheelset test rig based on the behaviour of the traction motor. Vehicle System Dynamics, 50 (8). pp. 1173-1185. ISSN 0042-3114

This version is available at http://eprints.hud.ac.uk/id/eprint/17452/

Re-adhesion control for rail vehicle traction based on the behaviour of the traction motor

Yunshi Zhao. Bo Liang

Institute of Railway Research, University of Huddersfield, Huddersfield, UK

Institute of Railway Research, University of Huddersfield, Queensgate, Huddersfield, UK, HD45AD

Y.Zhao@hud.ac.uk, B.Liang@hud.ac.uk

Provide short biographical notes on all contributors here if the journal requires them.

Re-adhesion control for rail vehicle traction based on the behaviour of the traction motor

A method for detecting wheel slip/slide and re-adhesion control of AC traction motors in railway applications is presented in this paper. This enables a better utilization of available adhesion and could also reduce wheel wear by reducing high creep values. With this method, the wheel – roller creepage, creep force and friction coefficient can be indirectly detected and estimated by measuring the voltage, current and speed of the AC traction motor and using an extended Kalman filter. The re-adhesion controller is designed to regulate the motor torque command according to the maximum available adhesion based on the estimated results. Simulations under different friction coefficients are carried out to test the proposed method.

Nomenclature

$\mathbf{A}$	System matrices for the induction motor
a, b	The contact ellipse semi-axes
C_{11}	longitudinal Kalker's coefficients
B, D	Reduction factors for the friction coefficient
F_N	Normal force at the wheel-roller surface
F_γ	Longitudinal creep force at the wheel-roller surface
$\mathbf{H}$	Measurement matrix for the induction motor at the motor
$I_{\alpha s}$, $I_{\beta s}$, $I_{\alpha r}$, $I_{\beta r}$	Stator and rotor current at α and β phase at the motor
i	Transmission ratio of the gearset
J_{motor}, J_{wheel}, J_{roller},	Inertia of the motor, wheel and roller
$\mathbf{K}$	Kalman filter gain matrix
k_A, k_S	Reduction factors of creep force
n_p	Number of poles of the motor

P⁻, P	Predicted and corrected error covariance matrix
Q, R	Covariance matrix of system noise and measurement noise
R_s, R_r	Stator and rotor resistances
R_{wheel}, R_{roller}	Radius of the wheel and roller
T_e	Electric torque of the motor
$U_{\alpha s}$, $U_{\alpha s}$, $U_{\alpha s}$, $U_{\alpha s}$	Stator and rotor voltage at α and β phase at the motor
V	Equivalent forward speed of the wheel
v	Measurement noise
w	System noise
ω_{motor}, ω_{wheel}, ω_{roller}	Rotating speed of the motor, wheel and roller
x	State variables
z	Measurements
$\hat{x}$, $\hat{x}^-$	Predicted and corrected state variables
γ	Creepage
μ, μ_0	Traction and friction coefficients
$\psi_{\alpha s}$, $\psi_{\beta s}$, $\psi_{\alpha r}$, $\psi_{\beta r}$	Stator and rotor flux at α and β phase at the motor

1. Introduction

In railway vehicle traction systems, it is necessary to reduce the occurrences of the excessive creepage between the wheel-rail surfaces to avoid wheel slip/slide and a decrease in traction effort, plus possible worse riding comfort, increase in wheel wear and noise. Large creep mostly occurs when the applied tractive effort exceeds the maximum available adhesion, during acceleration or deceleration. This phenomenon occurs more commonly when the wheel-rail surfaces are wet or contaminated with oil or leaves, as the friction coefficient may drop to very low levels.

To avoid this issue, re-adhesion control strategy has been studied and many different algorithms have been proposed [1-9]. In these algorithms, the vector control method is most commonly adopted, while the major differences lie in the way of detecting creepage and generating the torque command.

Yasuoka et al [1] presented a method in which slip is detected by comparing the speed difference between the wheel and the vehicle body (estimated by averaging the speed of all its axles).Then a torque compensation signal is generated using the estimated slip. Kim et al [2] suggested a model based re-adhesion control which treats the creep force as the mechanical load of the traction motor and the creepage force is estimated by a Kalman filter. Matsumoto [3] and Kawamura [4] investigated a single-inverter for multiple-induction-motors drive system, which uses the estimated adhesion force to adjust the torque commend and suppress the slip. The advantages for these applications are that they can regulate the traction system to work around the peak of the creepage – creep force curve, but require the knowledge of the friction coefficient and the vehicle speed, which are both hard to be measured accurately. Kadomaki et al [5] and Shimizu [6] evaluated anti-slip re-adhesion control based on speed-sensorless vector control and disturbance observer technique with a similar principal with the previously discussed work. However, it is questionable about the reliability of the sensorless control as its fundamental assumption is that the traction motor flux as constant which is only valid in certain cases. Spiryagin et al [7, 8] included the complex relationship between the creepage and creep force in the observers in his proposed method, to improve the results of pervious research. The friction coefficient is assumed to be measurable from wheel – rail noise and the vehicle speed is measurable by the GPS. Then the re-adhesion controller is proposed using the normal load, friction coefficient, vehicle and wheel speed to estimate the actual creep force, hence generating

the control commands which achieves its optimum performance. Mei [9] used the wheelset torsion vibration analysis to detect slip between wheel and rail which has an advantage of eliminating effort in the estimation of creepage and creep force using state observers. Iwnicki and Allen [10, 11] made some investigations about creep forces developed in the contact patch using roller rig. A model was suggested to calculate the wheel and rail creep force.

This paper presents a new approach estimating the creepage, creep force and friction coefficient between the wheel and rail surfaces with extended Kalman filter using the stator voltage, current and speed of the traction AC motor. The optimum operating point of the system is determined using the estimated friction coefficient. A torque compensation value is generated by comparing the estimated and desired electric torque. A wheel – roller dynamic model is built to apply and test the observer and controller. Polach's model is used describe the wheel – roller behaviour.

2. Traction system modelling

The simulated system used in this research is shown in Figure 1. In this system, a wheelset with two wheels is driven by an AC induction motor through a gear set. A pair of rollers is mounted under the wheels and driven by the creep forces generated at the contact patch between the wheels and rollers. Hence the dynamic equations are given as:

$$\frac{d}{dt}\omega_{motor} = \frac{T_e - 2\mathrm{iR}_{wheel}F_\gamma}{\mathrm{J}_{eqv}} \tag{2-1}$$

$$\omega_{wheel} = \frac{\omega_{motor}}{\mathrm{i}} \tag{2-2}$$

$$\frac{d}{dt}\omega_{roller} = \frac{2\mathrm{R}_{roller}F_\gamma}{\mathrm{J}_{roller}} \tag{2-3}$$

where $J_{eqv} = J_{motor} + \dfrac{J_{wheel}}{i^2}$

T_e is calculated using the traction motor model in a stationary α - β frame. Stator current and rotor flux are the state variables and the equations are list in Equation (2-4) to (2-7). The motor is controlled by an indirect flux oriented scheme [12], which is commonly used in railway traction and other applications.

$$\frac{d}{dt}I_{\alpha s} = -(\frac{R_s}{\sigma L_s} + \frac{1-\sigma}{\sigma t_r})I_{\alpha s} + \frac{L_m}{\sigma L_s L_r t_r}\psi_{\alpha r} + \frac{L_m}{\sigma L_s L_r}\omega_r\psi_{\beta r} + \frac{1}{\sigma L_s}U_{\alpha s} \qquad (2\text{-}4)$$

$$\frac{d}{dt}I_{\beta s} = -(\frac{R_s}{\sigma L_s} + \frac{1-\sigma}{\sigma t_r})I_{\beta s} - \frac{L_m}{\sigma L_s L_r}\omega_r\psi_{\alpha r} + \frac{L_m}{\sigma L_s L_r t_r}\psi_{\beta r} + \frac{1}{\sigma L_s}U_{\beta s} \qquad (2\text{-}5)$$

$$\frac{d}{dt}\psi_{\alpha r} = \frac{L_m}{t_r}I_{\alpha s} - \frac{1}{t_r}\psi_{\alpha r} - \omega_r\psi_{\beta r} \qquad (2\text{-}6)$$

$$\frac{d}{dt}\psi_{\beta r} = \frac{L_m}{t_r}I_{\beta s} + \omega_r\psi_{\alpha r} - \frac{1}{t_r}\psi_{\beta r} \qquad (2\text{-}7)$$

where $\sigma = 1 - \dfrac{L_m^2}{L_s L_r}$ and $t_r = \dfrac{L_r}{R_r}$

In this research, wheel – roller creep force F_γ is modelled based on the equations developed by Polach [13, 14]. In this method, the creep force is calculated by:

$$F_\gamma = \frac{2F_N\mu}{\pi}(\frac{k_A\varepsilon}{1+(k_A\varepsilon)^2} + \arctan(k_s\varepsilon)) \qquad (2\text{-}8)$$

and for the case of the longitudinal force

$$\varepsilon = \frac{G\pi abC_{11}}{4F_N\mu}\gamma \qquad (2\text{-}9)$$

k_A and k_S are the reduction factors regarding to the different conditions between the wheel and roller surface. k_A is related to the area of adhesion, k_S is related to the area of slip and $k_S \leq k_A \leq 1$.

In this model, it is considered that the traction coefficient depends on the slip velocity and friction coefficient, which is expressed by the following equation [14]

$$\mu = \mu_0((1-D)e^{-B\gamma V} + D) \tag{2-10}$$

$$V = 0.5(R_{roller}\omega_{roller} + R_{wheel}\omega_{wheel}) \tag{2-11}$$

The creep curves with different friction coefficient are plotted in Figure 2 and the optimum creepages (γ_{opt}) which achieve maximum creep forces are also marked out. In this simulation case, the normal force is 5kN and the forward speed is 10m/s. The values of B, D, k_A and k_S under different friction coefficient are listed in Table 1.

As the lateral dynamics of the system is not considered in this research, the creepage terms contains the longitudinal component only. The creepage is calculated by the following equation:

$$\gamma = 2\frac{R_{roller}\omega_{roller} - R_{wheel}\omega_{wheel}}{R_{roller}\omega_{roller} + R_{wheel}\omega_{wheel}} \tag{2-12}$$

3. State observer design

3.1 Extended Kalman filter

An Extended Kalman filter (EKF) is used to estimate the friction coefficient between the wheel and roller surfaces. EKF is the nonlinear version of the Kalman filter which linearizes about the estimation of the current mean and covariance using Taylor expansions.

A general scheme of an EKF estimation system is shown in Figure 3. The EKF is constructed based on the dynamic relationship which is used in the simulation model. The EKF estimates state variables of the simulation model using its inputs and measurements.

The state equation and measurement equation are given as:

$$x_{k+1} = \mathbf{A}x_k + w_k \tag{3-1}$$

$$z_k = \mathbf{H}x_k + v_k \tag{3-2}$$

where:

$$x = \left[I_{\alpha s}, I_{\beta s}, \psi_{\alpha r}, \psi_{\beta r}, \omega_{motor}, U_{\alpha s}, U_{\beta s}, \gamma, F_\gamma, \omega_{roller}, \mu, \mu_0 \right]^T \tag{3-3}$$

$$z = \left[I_{\alpha s}, I_{\beta s}, \omega_r, U_{\alpha s}, U_{\beta s} \right]^T \tag{3-4}$$

State matrix $\mathbf{A}$ and Measurement matrix $\mathbf{H}$ are determined by system dynamic equations (2-1) to (2-12). As the dynamic equations are nonlinear, extended Kalman filter is chosen to provide estimations of the state variable.

The EKF has a same 'prediction-correction' algorithm of the Kalman filter but linearize the state and observer matrix at each step of prediction and correction by calculating their Jacobian matrices of partial derivatives. The equations used in the EKF algorithm are listed in equation (3-5) to (3-9).

$$\hat{x}_{k+1}^- = \mathbf{A}\hat{x}_k \tag{3-5}$$

$$\mathbf{P}_{k+1} = \nabla \mathbf{A} \mathbf{P}_k \nabla \mathbf{A}^T + \mathbf{Q} \tag{3-6}$$

$$\mathbf{K}_k = \mathbf{P}_k^- \nabla \mathbf{H}^T (\nabla \mathbf{H} \mathbf{P}_k^- \nabla \mathbf{H}^T)^{-1} \tag{3-7}$$

$$\hat{x}_k = \hat{x}_k^- + \mathbf{K}_k(z_k - \mathbf{H}(\hat{x}_k^-)) \qquad (3\text{-}8)$$

$$\mathbf{P}_k = (\mathbf{I} - \mathbf{K}_k \nabla \mathbf{H})\mathbf{P}_k^- \qquad (3\text{-}9)$$

where $\mathbf{I}$ is an unit matrix, symbol ^ stands for estimated parameters and symbol ∇ is the Laplace operator.

3.2 Estimation result

The behaviour of the model discussed above has been simulated to prove the validity of the model and to provide measurements and other required parameters for the estimation which follows. The parameters of the system are given as: L_m=0.361H, L_s=0.362H, L_r=0.362H, R_s=3.2Ω, R_r=2.2Ω, R_{wheel}=0.1m, R_{roller}=0.2m, i=3, J_{wheel}=0.895Nm^2, J_{roller}=0.895Nm^2, F_N=5kN. Parameters B, D, k_A and k_S are selected according to Table 1. ψ_r^* is given as 5Wb and ω_{motor}^* changes by the following pattern:

$$\omega_{motor}^*(\text{rad/s}) = \begin{cases} 2\pi & t < 0.5\text{s} \\ 3\pi & 0.5\text{s} \le t < 1\text{s} \\ 2\pi & 1\text{s} \le t < 1.5\text{s} \\ 3\pi & 1.5\text{s} \le t < 2\text{s} \\ 2\pi & 2\text{s} \le t < 2.5\text{s} \\ 3\pi & 2.5\text{s} \le t < 3\text{s} \\ 2\pi & 3\text{s} \le t \le 3.5\text{s} \end{cases} \qquad (3\text{-}10)$$

where symbol * stands for control commands

While the friction coefficients are set according to the following equation to simulate 3 different contact conditions between the wheel and roller, which are dry, wet and low, as listed in Table 1.

$$\mu_0 = \begin{cases} 0.55 & t \le 1.2\text{s} \\ 0.3 & 1.2\text{s} < t \le 2.2\text{s} \\ 0.06 & 2.2\text{s} < t \le 3.5\text{s} \end{cases} \qquad (3\text{-}11)$$

The value of matrices $\mathbf{Q}$ and $\mathbf{R}$ can have a very large influence on the EKF performance. In this simulation, both of these matrices are assumed to be diagonal to reduce computing time. Both of these matrices should be obtained by considering the stochastic properties of the corresponding noises [15]. Due to the uncertainty of the system and measurement noise, $\mathbf{Q}$ and $\mathbf{R}$ are usually determined by the trial-and-error process. For this simulation, $\mathbf{Q}$ and $\mathbf{R}$ are set as:

$\mathbf{Q}$=diag{1e-6,1e-6,1e-6,1e-6,1e-6,1e-6,1e-6,1e-2,1e-2,1e-2,1e-2,1e-2}

$\mathbf{R}$=diag{1e-6,1e-6,1e-6,1e-6,1e-6}

State variables $\psi_{\alpha r}$, $\psi_{\beta r}$, and hence T_e are estimated from the EKF, as:

$$\hat{T}_e = \frac{\text{PL}_\text{m}}{\text{L}_\text{r}} (I_{\beta r}\hat{\psi}_{\alpha r} - I_{\alpha r}\hat{\psi}_{\beta r}) \qquad (3\text{-}12)$$

The estimation result and error are as follow. It can be seen that the error is generally small despite when the speed command suddenly changes and will only last a few time steps.

$\hat{\gamma}$ and $\hat{F}_\gamma$ are shown in Figure 5 and Figure 6 also shares a same pattern as the electric torque result, which only have remarkable error during the transition of the speed command.

In Figure 7, it can be seen that the estimated friction coefficient does not respond to the change of the actual value immediately but only changes when a large creepage occurs. This is due to the fact that the value of the creep force, hence the roller speed and the creepage are not affected by the traction coefficient unless the creepage is large

enough so that the creepage – creep force relationship reaches its saturation zone. However, this delay does not harm its performance for re-adhesion control, as the re-adhesion controller is only needed when large creepage occurs. Therefore an re-adhesion control scheme is developed using this estimation method, which is discussed in the next section.

4 Re-adhesion controller

4.1 Controller design

The block diagram of the proposed control scheme is presented in Figure 8. It is a typical IFOC diagram with an additional re-adhesion controller which is included in the dashed lines. The aim of applying this re-adhesion controller is to keep the system working at the peak of the creepage – creep force curve as shown in Figure 2. To achieve this, first the stator voltage and current signals of the motor is transformed to the α – β frame from the ABC frame, providing the information required by the extended Kalman filter block. Together with the voltage and current signals, motor speed is also fed into the EKF which estimates the creepage, creep force and traction coefficients. Finally the re-adhesion algorithm is applied thus compensate the electric torque command according to estimation results.

The re-adhesion algorithm is shown in Figure 9. In this algorithm, first the upper and lower limits of electric torque command are calculated according to the motor speed, the estimated traction coefficient and the optimized creepage (as shown in Figure 2) with the following equations:

$$T_{e\_limit} = \frac{R_{wheel}}{i} F_{opt} + J_{eqv}\dot{\omega}_r \qquad (4\text{-}1)$$

11

$$F_{opt} = \frac{2F_N\hat{\mu}}{\pi}\left(\frac{k_A\dfrac{G\pi abC_{11}}{4F_N\hat{\mu}}\gamma_{opt}}{1+(k_A\dfrac{G\pi abC_{11}}{4F_N\hat{\mu}}\gamma_{opt})^2} + \arctan(k_s\frac{G\pi abC_{11}}{4F_N\hat{\mu}}\gamma_{opt})\right) \qquad (4\text{-}2)$$

To keep the simplicity of the controller, the optimized creepage for friction coefficients other than those listed in Table 1 are determined using linear interpolation. As the main purpose of the controller is to avoid excessive creepage between the wheel and roller, it is not necessary to keep the wheel-roller creepage at its exact optimal value.

The command saturator block resets the value of T_e^* to its limitation when it is out of bounds. Then the error between the regulated electric torque command and the estimated electric torque will be fed into a PI regulator, to gain a smooth and stable performance.

4.2 Controller performance evaluation

Adding the re-adhesion controller in the loop, another simulation is carried out under the same conditions which are listed in section 3.

Figure 10 shows the wheel speed with and without the re-adhesion controller. When the re-adhesion controller is applied, the wheel speed changes much more slowly and smoothly. When the friction coefficient drops to its very low value, the influence of the controller on the wheel speed is more significant, as the the available adhesion between the wheel and roller are greatly reduced.

Though the wheel speed increases more slowly with the controller, the roller speed increase slightly faster as the controller regulates the creepage to its optimise value which can generate the maximum creep force, as shown in Figure 11.

The effect of the controller is very obvious in Figure 12, where the creepage difference is remarkable when the controller is applied. For the normal IFOC method,

the creepage could reach up to 60%, while the optimised value is no larger than 5.5%. The excessive creepage would lead to a large drop in the traction coefficient, therefore reducing the available creep force.

The utilization rate of the creep force can also increase with the use of controller, which explains why the roller speed increases faster when the controller is used, as presented in Figure 13.

Figure 14 shows that how much the creep force decreases with large creepage without the re-adhesion controller, while the creep force stays at a much larger value when the controller is engaged.

5 Conclusion

In this paper, an extended Kalman filter (EKF) based re-adhesion controller is proposed. First the EKF performance is evaluated in Section 3 by comparing the actual and estimated value of the electric torque, creepage, creep force and traction coefficient. In Section 4, the wheel – roller behaviour under the acceleration and deceleration is compared with or without the developed controller, showing that the creepage can be remarkably reduced, resulting in the increased traction coefficient and increased maximum adhesion furthermore. Therefore, the roller speed can respond faster with the controller, which shortens the traction and braking time. Moreover, the controller could also prevent wear of the wheel and rail by reducing the creepage.

Experiments will be carried out to test and adjust the proposed method on a 1/5 scaled roller rig in the future work. Lateral dynamics of the vehicle will also be included in the estimator.

Reference

[1]   I. Yasuoka*, et al.*, "Improvement of re-adhesion for commuter trains with vector control traction inverter," in *Power Conversion Conference-Nagaoka 1997., Proceedings of the*, 1997, pp. 51-56.

[2]   W. S. Kim*, et al.*, "Electro-mechanical re-adhesion control simulator for inverter-driven railway electric vehicle," in *Industry Applications Conference, 1999. Thirty-Fourth IAS Annual Meeting. Conference Record of the 1999 IEEE*, 1999, pp. 1026-1032.

[3]   Y. Matsumoto*, et al.*, "Novel re-adhesion control for train traction system of the," in *Industrial Electronics Society, 2001. IECON'01. The 27th Annual Conference of the IEEE*, 2001, pp. 1207-1212.

[4]   A. Kawamura*, et al.*, "Measurement of tractive force and the new maximum tractive force control by the newly developed tractive force measurement equipment," *Electrical Engineering in Japan,* vol. 149, pp. 49-59, 2004.

[5]   S. Kadowaki*, et al.*, "Antislip readhesion control based on speed-sensorless vector control and disturbance observer for electric commuter train—Series 205-5000 of the East Japan Railway Company," *Industrial Electronics, IEEE Transactions on,* vol. 54, pp. 2001-2008, 2007.

[6]   Y. Shimizu*, et al.*, "Anti‐slip/slid re‐adhesion control based on disturbance observer considering bogie vibration," *Electrical Engineering in Japan,* vol. 172, pp. 37-46, 2010.

[7]   M. Spiryagin*, et al.*, "Control system for maximum use of adhesive forces of a railway vehicle in a tractive mode," *Mechanical systems and signal processing,* vol. 22, pp. 709-720, 2008.

[8]   M. Spiryagin*, et al.*, "Development of traction control for hauling locomotives," *Journal of System Design and Dynamics,* vol. 5, pp. 1214-1225, 2011.

[9]   T. Mei*, et al.*, "A mechatronic approach for effective wheel slip control in railway traction," *Proceedings of the Institution of Mechanical Engineers, Part F: Journal of Rail and Rapid Transit,* vol. 223, pp. 295-304, 2009.

[10]   P. Allen and S. D. Iwnicki, "The critical speed of a railway vehicle on a roller rig," *Proceedings of the Institution of Mechanical Engineers, Part F: Journal of Rail and Rapid Transit,* vol. 215, p. 55, 2001.

[11]   S. Iwnicki, "Simulation of wheel–rail contact forces," *Fatigue & Fracture of Engineering Materials & Structures,* vol. 26, pp. 887-900, 2003.

[12]   B. K. Bose, *Modern power electronics and AC drives*: Prentice Hall PTR, 2002.

[13]   O. Polach, "A fast wheel-rail forces calculation computer code," *Vehicle System Dynamics,* vol. 33, pp. 728-739, 2000.

[14]   O. Polach, "Creep forces in simulations of traction vehicles running on adhesion limit," *Wear,* vol. 258, pp. 992-1000, 2005.

[15]   P. Vas, *Sensorless vector and direct torque control* vol. 729: Oxford university press Oxford, UK, 1998.

[16]   G. Charles and R. Goodall, "Low Adhesion Estimation," in *Railway Condition Monitoring, 2006. The Institution of Engineering and Technology International Conference on*, 2006, pp. 96-101.
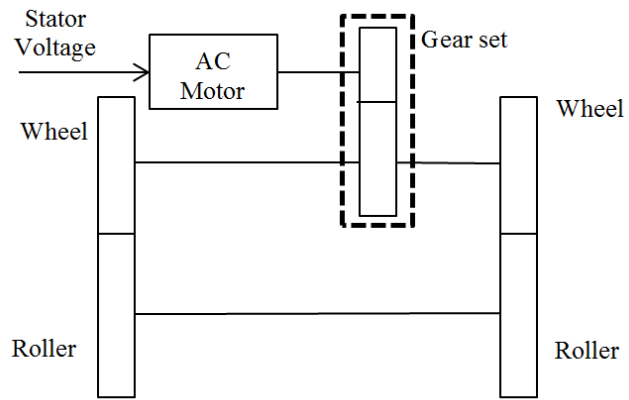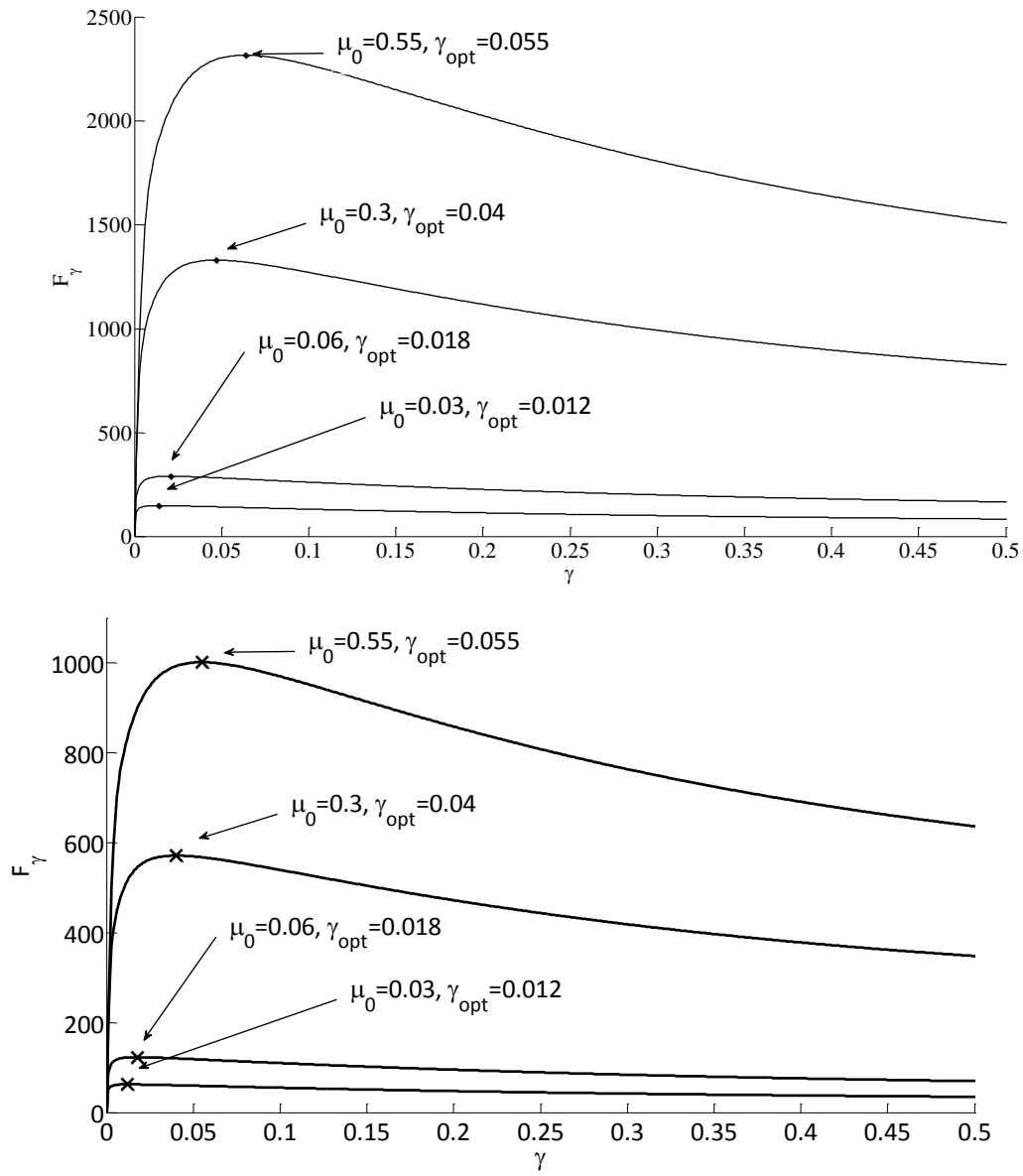
Figure 1 Block diagram of the simulated system

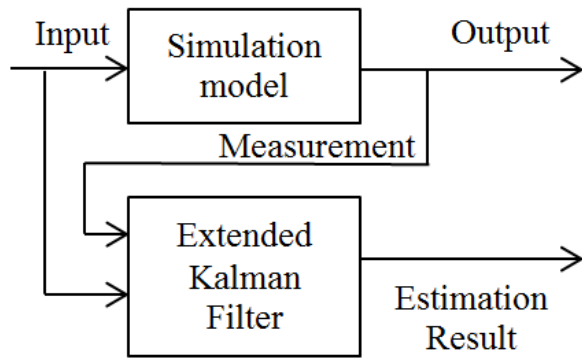Figure 2 Creepage-creep force curves with different friction coefficients

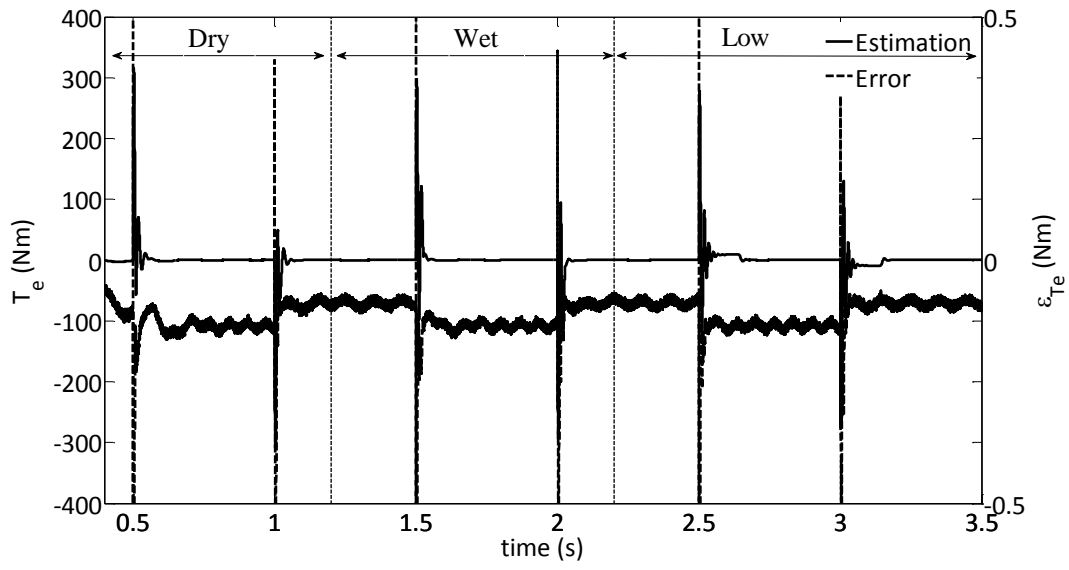Figure 3. Block diagram for the system estimation using Kalman filter.

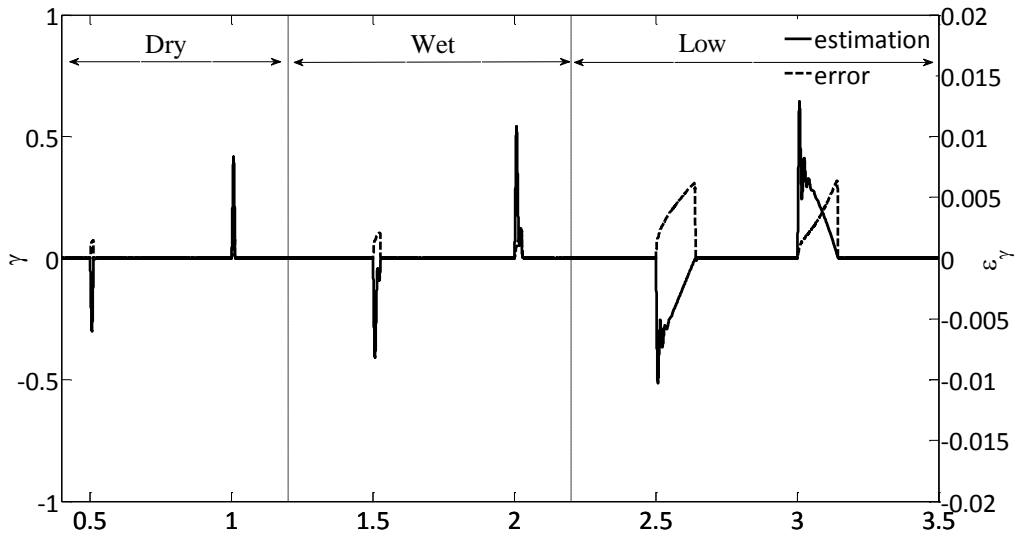Figure 4 Estimation and error of the electric torque
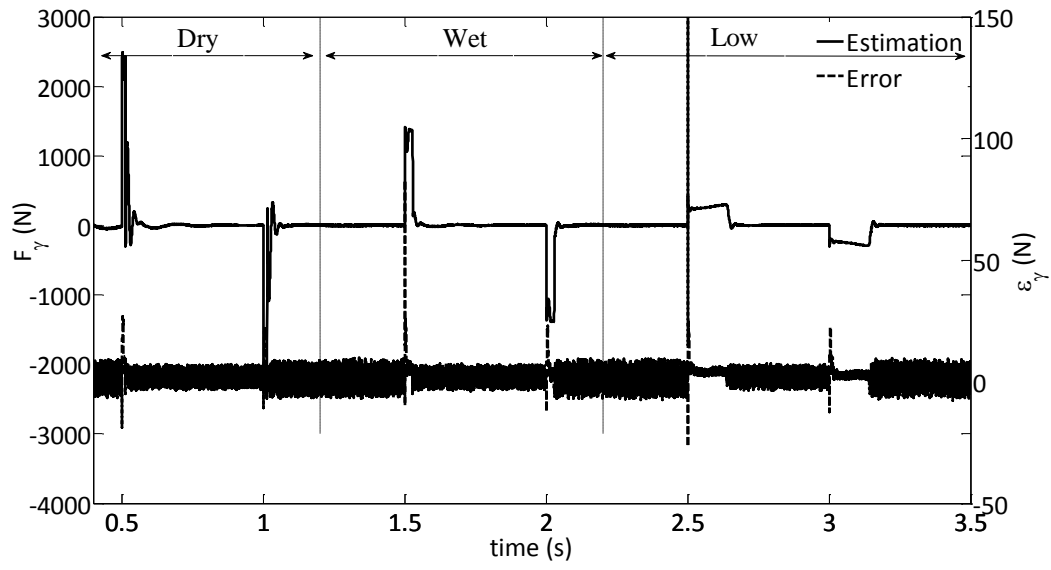
Figure 5 Estimation and error of the creepage
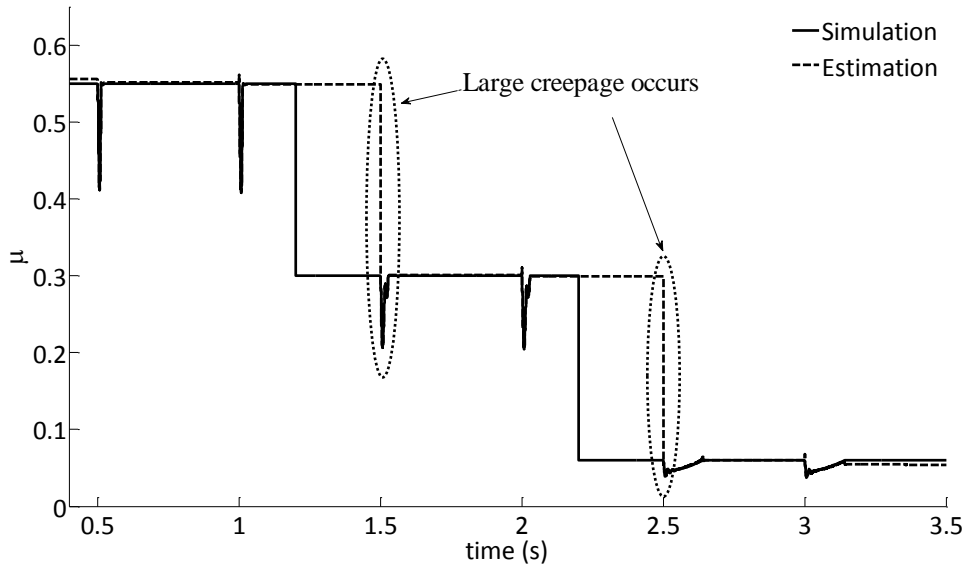
Figure 6 Estimation and error of the creep force

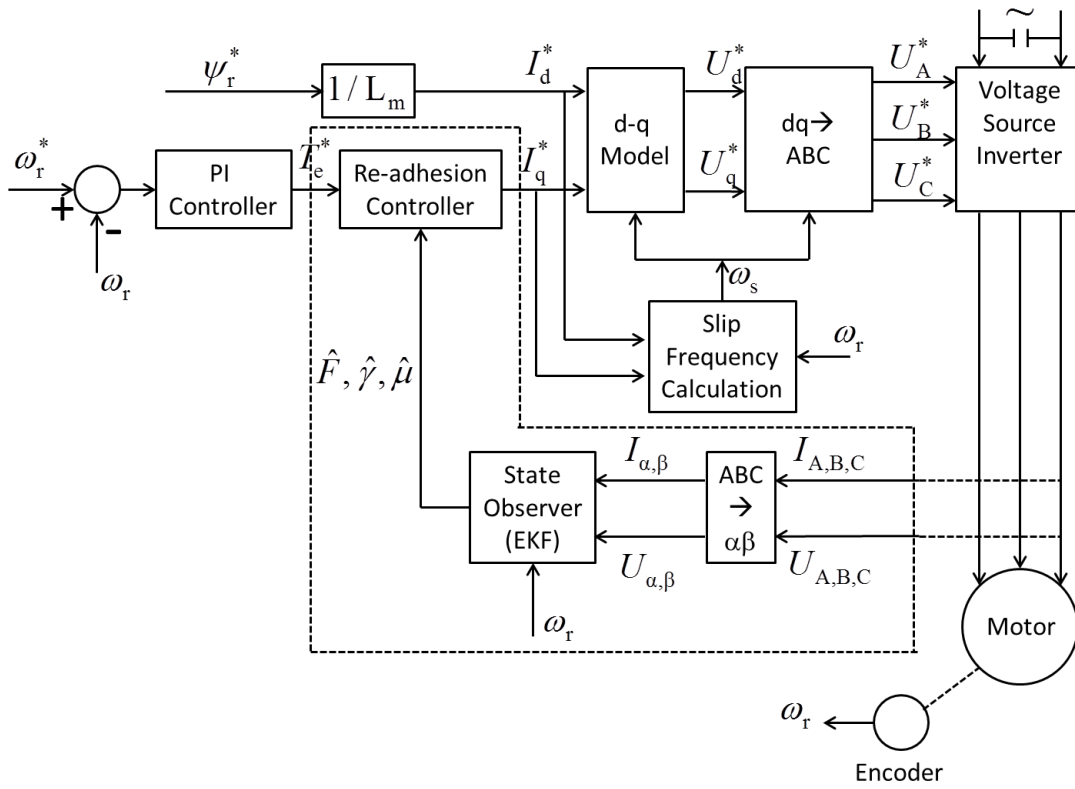Figure 7 Actual result and estimation of the traction coefficient

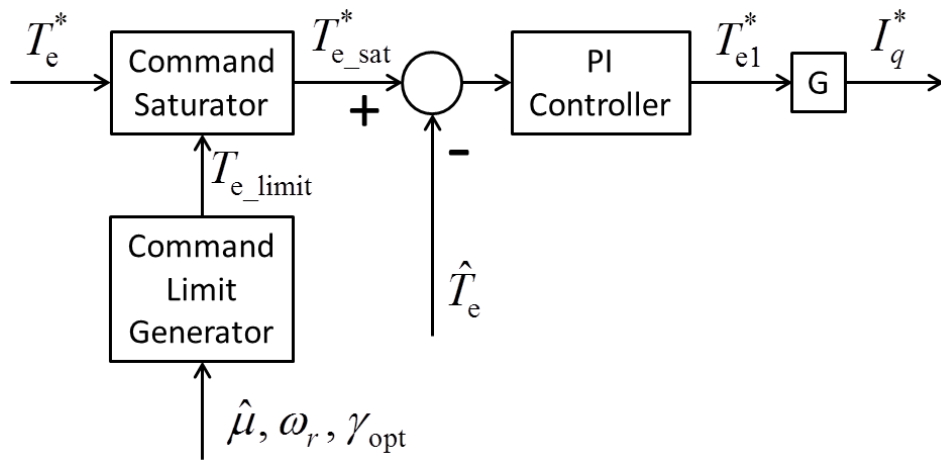Figure 8. Block diagram of the control scheme of the traction motor

Figure 9 Re-adhesion controller structure
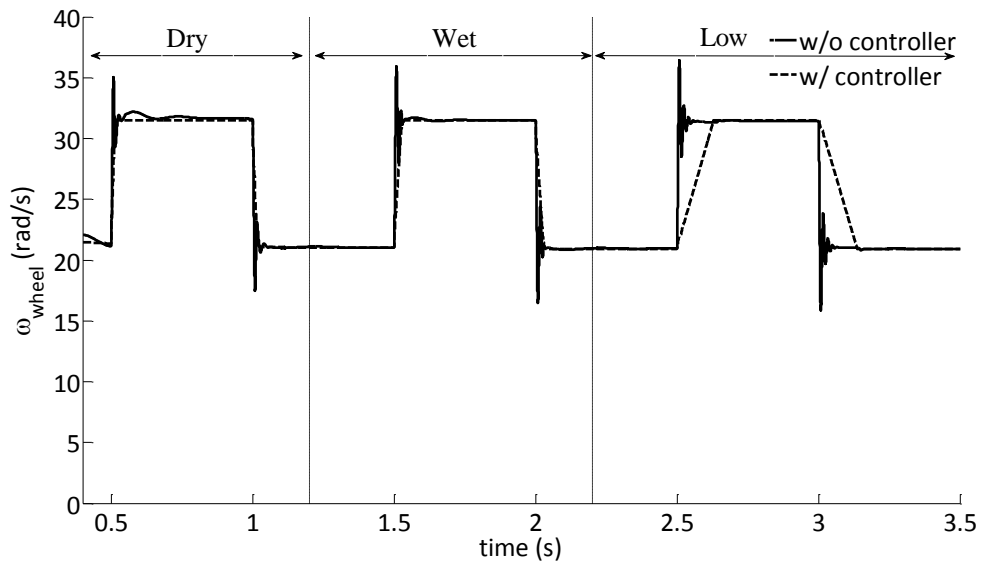
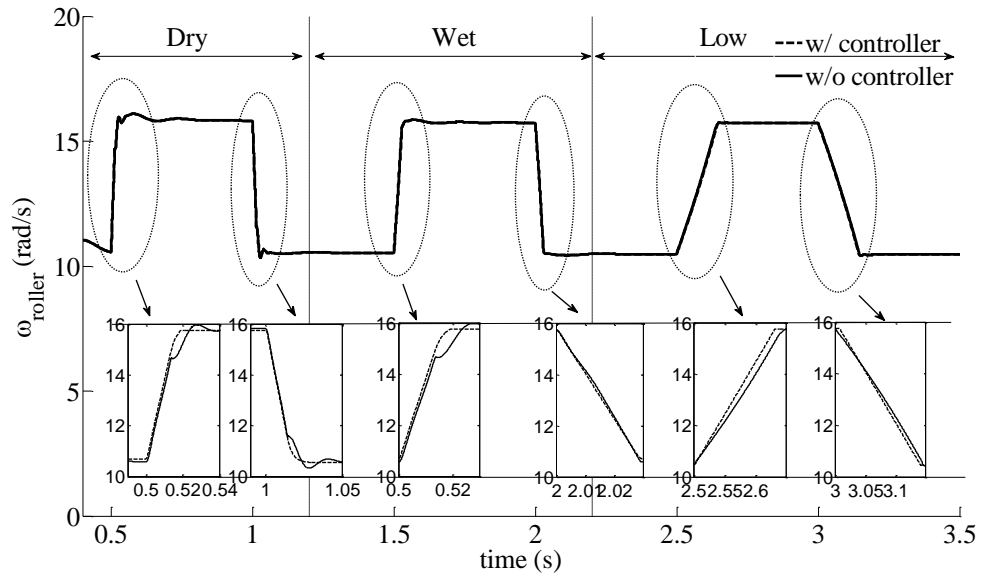Figure 10 Wheel speed performance with and without controller

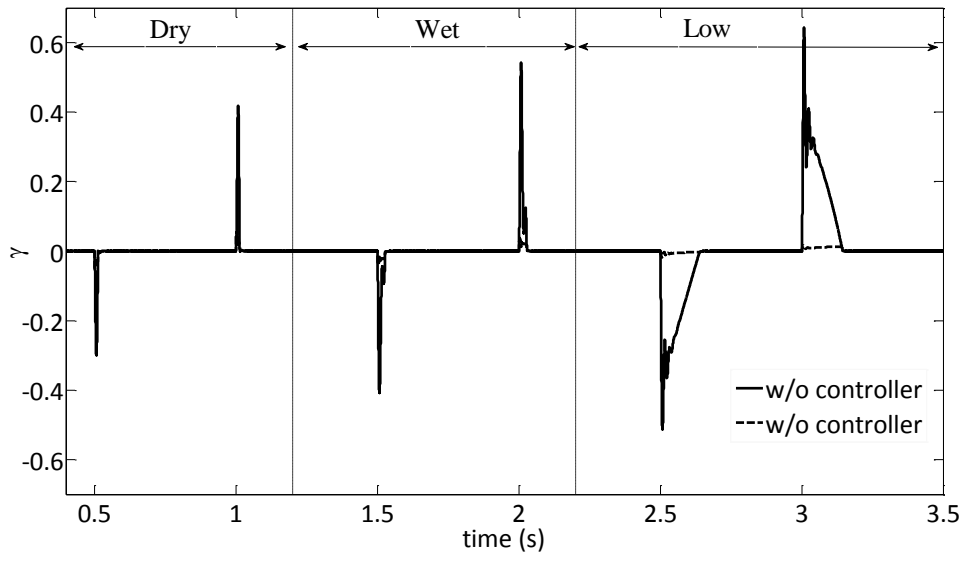Figure 11 Roller speed performance with and without controller

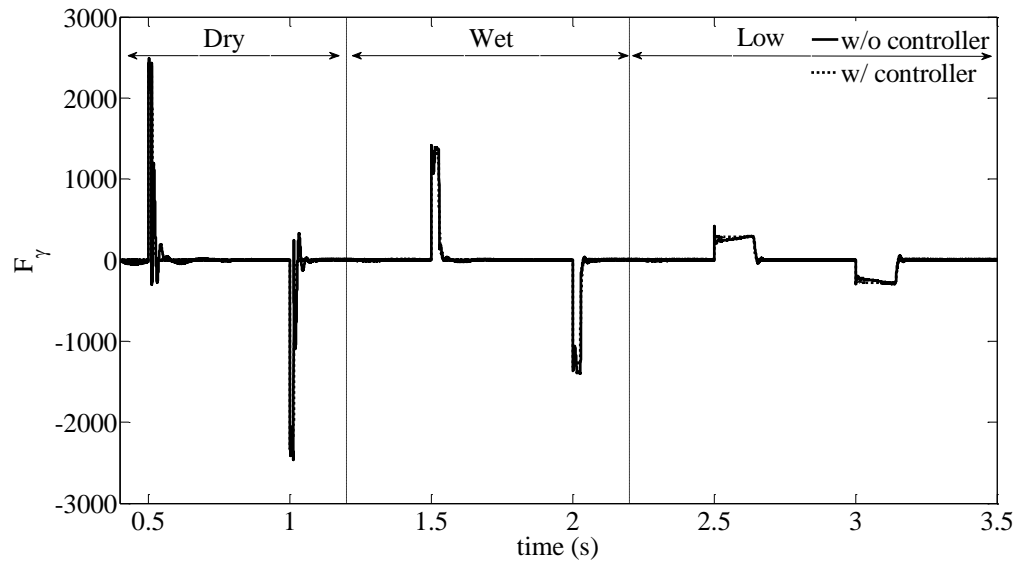Figure 12 Creepage performance with and without controller

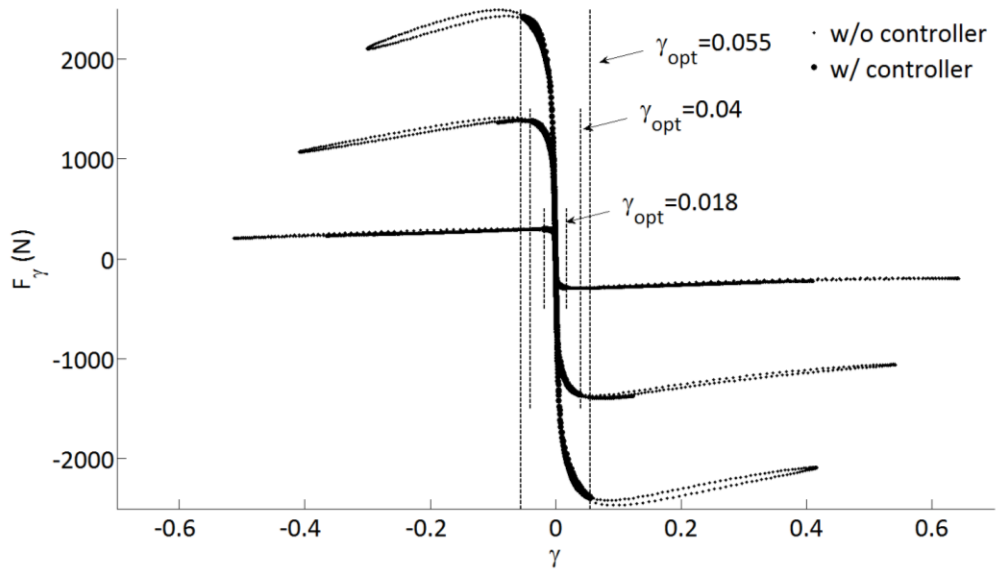Figure 13 Creep force performance with and without controller

Figure 14 Creepage – creep force with and without controller

Table 1 Parameters of Polach model under different friction coefficients [16]

Parameter	Dry	Wet	Low	Very Low
k_A	1.00	1.00	1.00	1.00
k_S	0.40	0.40	0.40	0.40
μ_0	0.55	0.30	0.06	0.03
B	0.40	0.40	0.40	0.40
D	0.60	0.20	0.20	0.10